

# Stable Haptic Interaction Using Passive and Active Actuators

Carlos Rossa, José Lozada, and Alain Micaelli

**Abstract**— This paper presents a stable control method for a hybrid haptic device comprising a brake and a motor. A review of stability condition via describing function analysis is first presented. The results show that while brakes are intrinsically stable, an active device is limited in terms of stiffness. The stability is however improved if the brake simulates a physical damping. Subsequently, the stability condition is obtained via passivity condition analysis. The results demonstrate that the stiffness is improved by engaging both actuators to create resistive forces and the passivity is respected assuming a passive virtual environment. An energy and a stiffness-bounding algorithms have been developed in order to assure the stability of the coupled system in this case. It has been tested and validated using a 1-DOF hybrid haptic device by the simulation of an unstable and an active virtual environments respectively. Experimental results show that the displayable stiffness is improved under stability conditions using the control method. Furthermore, it allows the hybrid system to simulate nonlinear and unstable virtual environments and the controller remains independent of the virtual environment model.

## 1. MOTIVATION

Haptic devices are a range of robotic systems designated to display reflecting forces to an human operator using mechanical actuators. By this means he is able to feel, touch and manipulate computer-generated environments or teleoperation tasks.

Stability and transparency are a key design requirement in haptic systems. The ideal haptic device possesses no inertia and friction, infinite bandwidth and should be able to vary from zero (complete freedom) to infinite (complete constraint) output impedance while maintaining stability.

The use of active actuators such as DC motors is amply widespread in the design of haptic devices since it can display reflecting forces with a relatively fast response time and good control performance. However, it is well-known that there is a compromise between the stability and the control loop gains [1]. As a consequence, any active haptic device will exhibit a finite dynamic range of impedance. Therefore, Colgate and Brown [2] introduced the concept of "Z-width" as the dynamic range of achievable impedance, and invoked factors affecting performance including the interface dynamics, sensors quantization and the sampling rate.

To achieve stable haptic interaction, several researchers paid attention to two main control methods: First, Colgate et al. [3] presented the concept of virtual coupling which bounds the range of achievable impedance for passive human

The authors are with the French Atomic Energy Commission - CEA, LIST, Sensorial and Ambient Interfaces Laboratory, 91191 Gif-sur-Yvette CEDEX, France. e-mail: [rossa@ualberta.ca](mailto:rossa@ualberta.ca); [joselozada@uti.edu.ec](mailto:joselozada@uti.edu.ec); [alain.micaelli@cea.fr](mailto:alain.micaelli@cea.fr).

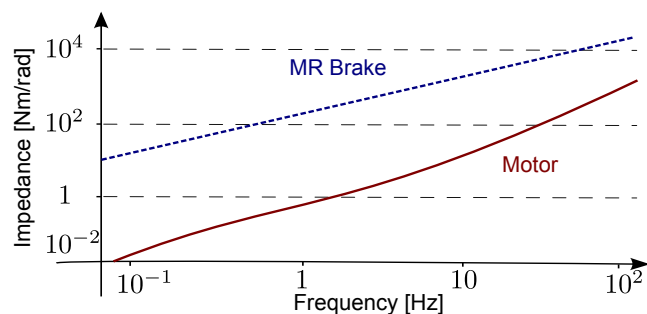


Fig. 1. Comparative analysis of displacement impedance range of a MR brake (Lord Corp. RD-2068-10, 5 Nm.) and a DC motor (Maxon EC-40, 220 mNm). The actuators are coupled to a reduction stage in order to obtain 50Nm at the end effector [10].

operators and environments. Adams and Hannaford [4] use two-port network theory to determine optimal virtual coupling parameters. The second method is based on the use of a passivity-based control schemes as a passivity controller that limits the restored energy to no more than the energy provided by the operator [5][6]. Although passivity-based control is an effective way to guarantee stability, it cannot assure the interface's fundamental safety.

The mentioned studies assume that the force reflecting is active and reach the consensus that for guaranteeing stability, some energy dissipation is necessary. Notwithstanding, active actuators can be replaced by passive actuators, which are intrinsically stable and safe. Compared with a conventional DC motor, magnetorheological (MR) brakes, for example, have the advantage of a higher torque/volume and torque/mass ratio and present lower power requirements. Furthermore, MR brakes provide greater mechanical impedance compared to a motor as presented in Fig. 1. Nonetheless, passive actuators cannot restore energy to the operator, and as a consequence, the haptic rendering is limited [7]. Therefore, an hybrid system comprising active and passive actuators appears as an encouraging solution to achieve both large Z-width and large stability ranges [8]. When the actuators are linked in parallel, the presence of a passive high torque density actuator allows the use of an active actuator with an inferior torque capacity. This configuration enhances the transparency of the device by removing, for example, the reduction stages [9].

Two main actuation approaches are employed for the control of hybrid actuators: When the motor is used to create the reflecting forces, the brake can display a controllable physical damping to provide for the motor's stability [11]. Conversely, in the second case where the rendering is assumed by the brake, the motor assists the brake by compensating for its inherent residual torque [12]. In the first case, the stability of

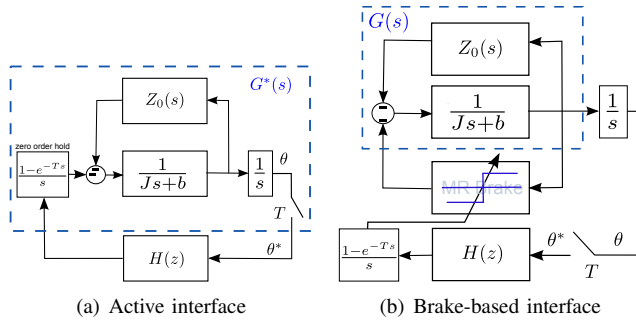


Fig. 2. Different kinds of force feedback devices: an active interface based on a conventional motor (a) and a passive interface comprising a controllable brake (b).

the system can be improved, but the stiffness remains limited by the torque capacity of the motor. In the second case, the actuation is based on the brake; the stiffness could be improved but the interface remains too conservative. These two methods turn out to be complementary, thus, another possibility is to activate the actuators independently. For instance, the brake and the motor could be used to create dissipative forces and the motor can also restore some energy to the operator.

This paper is organized as follows. An analysis of stability is performed using different approaches: In Section 2, the stability condition is obtained via describing function analysis. In Section 3, the brake is used to simulate a stiffness and the stability condition is obtained via passivity condition analysis. Subsequently, based on the stability constraints, an energy and a stiffness-bounding algorithms are presented. It has been tested and validated using a 1-DOF hybrid haptic device and the results are presented in Section 5.

## 2. STABILITY VIA DESCRIBING FUNCTION ANALYSIS

This analysis aims to highlight the influence of a controllable physical damping on the performance of an hybrid actuator.

The following example refers to Fig. 2. Consider a 1-DOF force-feedback interface composed of a mechanical device which has as an inertia  $J$  and some viscous friction  $b$ . The virtual environment is represented as a function  $H(z)$ , linear or not, which contains the mathematical model of the simulation and calculates the interaction torque  $\tau_h$  as a function of the end-effector position  $\theta^*$ . A human operator, modelled as a passive impedance  $Z_0(s)$ , interacts with the device. The system is controlled with a sampling rate  $T$  and the conversion between the discrete and continuous domain is obtained by a zero-order hold function  $ZOH(s) = \frac{1-e^{-Ts}}{s}$ .

The interface of Fig. 2(a) employs an active actuator while in 2(b) a passive one is used. The control loop scheme can be divided into two different subsystems. The first, called  $G(j\omega)$ , comprises the human operator, the haptic device and the actuator. The second is the virtual environment  $H(z)$ . The mechanical device, the human operator and the virtual environment are assumed to be strictly passive, it implies  $Re\{H(e^{sT})\} \geq 0$ ,  $Re\{Z_0(s)\} \geq 0$  and  $Re\{Js+b\} \geq 0$ . The characteristic equation of the transfer function in closed-loop is  $1+H(e^{sT})G(s) = 0$ . The solution to this equation is

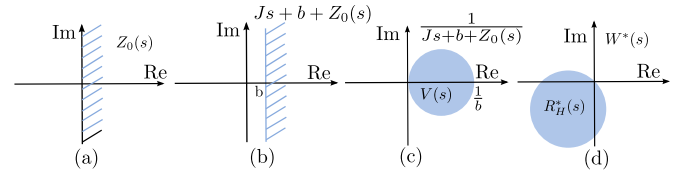


Fig. 3. Evolution of the Nyquist regions of the transfer function of an active and a passive interfaces.

given by the intersection between the correspondent Nyquist region of the function  $G(s)$  and the locus of  $-\frac{1}{H(e^{sT})}$ , which represents the limit cycles of stability. This analysis is presented in Fig. 3. Since the user's impedance is assumed to be passive, its Nyquist region occupies the right side in the Real/Imaginary plane (Fig. 3a). When combined to the impedance of the device, this region is shifted to the right by  $b$  units (Fig. 3b). The inverse of the total impedance takes the form of a closed disk  $V(s)$  with a radius  $1/2b$  (Fig. 3c).

Consider the passive interface presented in Fig. 2(b). The locus of the transfer function of the actuator and of the virtual environment occupies the right half plan of the complex plan. As a consequence, they will never be encircled by the region  $V(s)$  of the function  $1/(Js+b+Z_0(s))$ . In other words, there is no stability limit cycles.

Now, consider the active interface of Fig. 2(a). In this case, the  $ZOH(s)$  function creates a delay due to the sampling rate. It injects energy into the system in an amount proportional to the displayed force [13]. The Nyquist region of the transfer function of the user and of the mechanical device  $V(s)$  is shifted to the third quadrant (Fig. 3d) and is represented by the region denoted  $R_H^*(s)$ . Thus, for a given value of  $T$ ,  $\omega$  and  $b$ , there can be intersections between the Nyquist region of the active interface transfer function and the locus of  $-\frac{1}{H(e^{sT})}$ .

Colgate and Schenkel [1] obtained a stability criterion for the simulation of a virtual wall modelled as a spring-damper system with a stiffness  $K$  and a damping  $B$  given by:

$$b > \frac{TK}{2} + B \quad (1)$$

From this equation we can draw that to achieve stability some physical energy dissipation is necessary. Nevertheless, an inherent physical damping damages the transparency of the haptic rendering. A brake can then provide a controllable physical damping  $B$  varying from low to high output impedance. The passivity condition becomes  $b+B > Tk/2$  [14]. This approach can effectively improve the maximum stable stiffness of the motor but the total stiffness of the system remains globally limited by the torque capacity of the motor.

This analysis demonstrates that for an active interface there is a tradeoff between the stiffness and the stability. Another control possibility may consist of engaging both actuators to simulate a stiffness. With this goal in mind, an analysis of stability via passivity condition is conducted in the next section. Subsequently, an energy and stiffness-bounding algorithms are presented in order to guarantee the stability of the coupled system.



$0 < \beta(\tau_h) \leq 1$ , it implies  $S(u) [\beta(\tau_h) - 1] P(u) \geq 0$  and the interface is guaranteed to be passive.

Based on these statements, Section 4 presents a control method which aims to provide a stable interaction.

#### 4. STABLE CONTROL

In the previous sections, a stability analysis of a hybrid interface was developed. Via describing function analysis, it can be concluded that, in contrast to the motor, the brake is not limited in terms of displayable stiffness. Via passivity condition analysis, it has been shown that the system is maintained passive if the virtual environment is also passive. These two circumstances, when not respected, contribute to the instability of the system.

In this section, two algorithms are implemented in the controller in order to ensure the stability of the coupled system even for non-linear and unstable virtual environments. First, in order to maximize the reactivity of the hybrid system a control method is proposed. In view of assuring the passivity of the system when the passivity condition of the virtual environment is not respected, an energy-bounding based control method is subsequently implemented. The second method consists of a stiffness-bounding based control, which is able to limit the stiffness sent to the motor in order to assure the passivity condition obtained by describing function analysis.

##### 4.1 Energy-bounding Algorithm Definition

In order to determine an optimal shearing of the efforts between the brake and the motor, the observation of the power is used to determine if the interface should dissipate or restore energy. The brake can only be enabled to dissipate energy while the motor can display both active and dissipative behaviours.

By definition, the haptic device dissipates energy if the force applied by the interface on the operator is opposed to the velocity. The observed power is then positive. In other words, the power flows from the operator to the interface. Thus, if  $P < 0$ , the controller sets  $S(u) = 1$  and  $P \geq 0 \therefore 0 \leq S(u) \leq 1$ .

Using the power flow-based control, the controller needs only two pieces of information: the torque calculated by the virtual environment  $\tau_h^*$  and a measure of the position or velocity. It enables to decouple the design of the controller from that of virtual environments [15].

In order to obtain a transparent transition between the brake and the motor, and to maximize the reactivity of the system, the actuation approach works as follows. The motor is activated up to its saturation in both cases. Beyond this point, and for a dissipative behaviour, the torque is compensated by the brake so that  $\tau_b = \tau_h - \tau_{sat}$  if  $|\tau_h| > |\tau_{sat}|$ .

If the motor has a torque capacity, called  $\tau_{sat}$ , inferior to the brake, the unsaturation ratio of the motor  $\beta(\tau_h)$  can be computed as follows:

$$\beta(\tau_h) = \frac{\min(|\tau_h|, |\tau_{sat}|)}{|\tau_h|} \quad (8)$$

As a result the variable  $S(u)$  should be set to  $\beta(\tau_h)$  for a dissipative behaviour and to 1 when the interface restores energy. In order to implement this control method, a power-sign dependent variable  $\sigma(P) = 0$  if  $P(u) \geq 0$  and  $\sigma(P) = 1$  if  $P(u) < 0$ , is defined as:

$$\sigma(P) = \frac{1}{2} [\text{sgn}(P) - 1] \text{sgn}(P) \quad (9)$$

Thus, the variable  $S(u)$  can be computed as follows:

$$S(u) = \beta(\tau_h)(1 - \sigma(P)) + \sigma(P) \quad (10)$$

The torque provided by the motor can then be redefined as  $\tau_{mh} = S(u)ZOH\tau_h$  while the braking torque remains  $\tau_b = (1 - S(u))ZOH\tau_h$ .

The passivity condition is not respected if the virtual environment is not passive. Furthermore, the *ZOH* function injects energy into the system in an amount proportional to the displayable stiffness [13]. It may cause the violation of the stability criterion. However, the passivity of the system can be assured by the controller if a limitation of the active torque is implemented.

Since the brake cannot inject energy into the system, the energy-bounding algorithm is defined only as a function of the energy provided by the motor. Its energy is defined as  $E(n) = -\sum_{k=1}^n \tau_{mh}(k)\dot{\theta}(k)$ . Another possibility may consist of considering the energy of the coupled system  $E_c(n) = -\sum_{k=1}^n [\tau_{mh}(k) + \tau_b(k)]\dot{\theta}(k)$  as the passivity observer. However, if the brake has a greater torque capacity than the motor, the energy observer stores a high value of energy and the motor will not be constrained to display a passive behaviour up to the restitution of the total stored energy.

The controller works as follows. If the energy becomes negative, it means that the interface is not passive. The reference torque  $\tau_h$  is then transferred to the brake instead of the motor and the created energy is dissipated. In this case, there are two possibilities: if the user tries to turn the end-effector in the direction of the reference torque (the power is negative) the brake is activated by setting  $S(u) = 0$ ; if the interface dissipates energy, even if the energy observer is negative, the motor can again be activated by setting  $S(u) = \beta(\tau_h)$ . Taking into consideration the dissipated energy by the brake in this case, the energy observer can be defined as  $E(n) = -\sum_{k=1}^n [\tau_{mh}(k) + \tau_b(k)\sigma(P)]\dot{\theta}(k)$ .

The energy-bounding based control takes the following formulation:

$$S(u) = \begin{cases} \beta(\tau_h)(1 - \sigma(P)) + \sigma(P) & \text{if } E \geq 0 \\ \beta(\tau_h)(1 - \sigma(P)) & \text{otherwise} \end{cases} \quad (11)$$

The unsaturation ratio of the coupled system, called  $\alpha(u)$ , is computed as follows:

$$\alpha(u) = \sigma(P)(\beta(\tau_h) - 1) + 1 \quad (12)$$

The variable  $\alpha(u)$  indicates the capacity of the system to respect the reference torque. The evolution of the variables is presented in Fig. 5. The interface dissipates energy when  $P(u) \geq 0$ . Only the motor is activated up to its saturation by

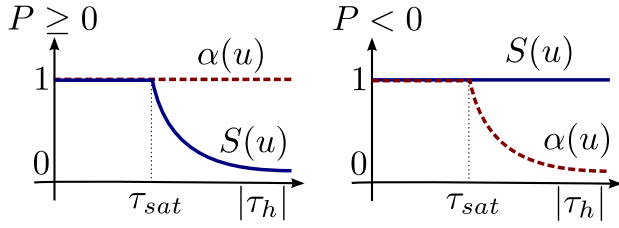


Fig. 5. Time-variant control variable  $S(u)$  and the unsaturation ratio of the system  $\alpha(u)$ . For a dissipative behavior both actuators are engaged and the system can display the required torque ( $\alpha(u) = 1$ ). For an active behavior only the motor is enabled if  $E \geq 0$ , the saturation of the system depends on the torque capacity of the motor.

setting  $S(u) = 1$ . Beyond this point, the brake compensates for the error between the reference torque and the saturation of the motor. Thus, both actuators are engaged at the same time and braking the torque increases as a function of  $S(u)$ . The system is able to dissipate all the energy of the virtual environment and  $\alpha(u) = 1$ . When  $P(u) < 0$  the interface restores energy to the operator. In this case only the motor can be engaged and  $S(u)$  is set to 1. The system displays the reference torque only up to the saturation of the motor ( $\alpha(u) = 1$  if  $\tau_h < \tau_{sat}$ ). Beyond this point the system becomes saturated and  $\alpha(u)$  decreases as a function of the reference torque.

Using this control method, the brake and the motor can be treated as two independent actuators. The total stiffness of the system is the contribution both of the stiffness of the motor and the brake. The only constraint is that if the energy of the motor is negative, the brake is enabled instead of the motor.

#### 4.2 Stiffness-bounding Algorithm Definition

According to the proposed control method, only the motor is engaged until its saturation. During this phase, the stiffness is limited according to the stability criterion of Section 2. The maximal stiffness  $k_{lim}$  under stability conditions is calculated by  $k_{lim} = 2\frac{b}{T}$ . The controller then compares the variation of the torque calculated by the virtual environment with the variation of the measured position called  $\delta\theta = \theta_{(k)} - \theta_{(k-1)}$  to deduce the stiffness of the virtual environment. If the stiffness violates the stability criterion, the effective torque sent to the motor, called  $\tau_{sb(k)}$ , should be recalculated and the difference sent to the brake. The index  $(k)$  represents the actual value of the variable and  $(k-1)$  is the value at the previous sampling time.

The stiffness bounding algorithm takes the following formulation:

$$\tau_{sb(k)} = \begin{cases} \tau_h(k) & \text{if } \frac{\tau_h(k) - \tau_{sb(k-1)}}{\delta\theta} \leq k_{lim} \\ k_{lim}\delta\theta + \tau_{sb(k-1)} & \text{otherwise} \end{cases} \quad (13)$$

For a dissipative behaviour, the difference between  $\tau_h$  and  $\tau_{sb}$  is compensated by the brake so that  $\tau_b(k) = \tau_h(k) - \tau_{sb(k)}$ . It is obtained by recalculating  $S(u)$ : Since  $\tau_b = ZOH(1 - S(u))\tau_h$ , it implies  $S(u) = \tau_{sb}/\tau_h$ . Taking into consideration the saturation of the motor, this condition can be achieved by redefining  $\beta(\tau_h)$  as:

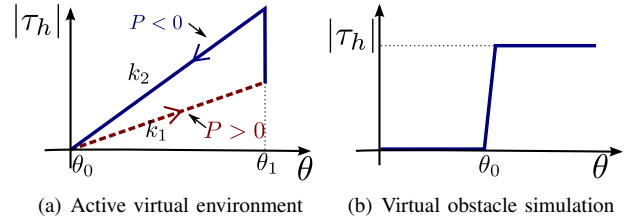


Fig. 6. Unstable virtual environments designed to validate the control algorithms: An active (a) and a high stiffness (b) models are used to validate the energy-bounding and the stiffness-bounding algorithms respectively.

$$\beta(\tau_h) = \frac{\min(|\tau_{sb}|, |\tau_{sat}|)}{|\tau_h|} \quad (14)$$

Where  $S(u)$  is defined by (11). Note that the algorithm is implemented in the controller and thereby the virtual environment is not altered.

## 5. EXPERIMENTAL RESULTS

A test bench composed of a Maxon motor RE40 with a maximal torque of 0.302Nm, linked in parallel to a Lord Corp. MR brake RD2078, maximal torque 2Nm, was used to validate the control laws (Fig. 7(a)). The system is controlled by a microcontroller (Silicon Lab. C8051F120) operating at 99.4MHz. The sampling rate is  $T=200\mu s$ . The angular position is measured using an incremental encoder with 500 pulses per revolution. Fig. 7(b) shows the control loop. The control laws are implemented in the controller and are independent of the virtual environment  $H(z)$ .

Two tests were conducted. In the first case, the passivity condition is obtained using the energy-bounding algorithm and in the second experiment the passivity condition is respected using the stiffness-bounding algorithm. To validate the control laws, the virtual environment has been defined as an active simulation and a virtual obstacle with high stiffness for each test respectively (Fig. 6).

### 5.1 Energy-Bounding Algorithm

The first virtual environment designed to validate the control laws simulates a variable-stiffness angular spring (Fig. 6(a)). The stiffness  $k_2$  during the decompression phase ( $P < 0$ ) is greater than the stiffness  $k_1$  during the compression phase ( $P > 0$ ). The energy of the spring is given by  $\int_0^\theta \tau_h d\theta$  with  $\tau_h = K\theta$ . For two different stiffness, the total energy of the simulation, if the end-effector compresses the spring and returns to the initial position, is given by  $E_{ve} = \int_{\theta_0}^{\theta_1} k_1\theta d\theta + \int_{\theta_1}^{\theta_0} k_2\theta d\theta$ . If  $k_2 > k_1$ ,  $E_{ve} < 0$  and the passivity condition is not be respected: the virtual environment creates energy and the amount of created energy is  $-E_{ve}$ . It enables the simulation to observe the impact of an active virtual environment in the passivity condition. Consider  $k_2 = 10k_1$ .

The experimental result is shown in Fig. 8. The end-effector attains the spring at  $t=0.38s$  (A). The virtual environment then calculates a torque opposed to the velocity. It represents a dissipative behaviour ( $P > 0$ ). The motor follows the

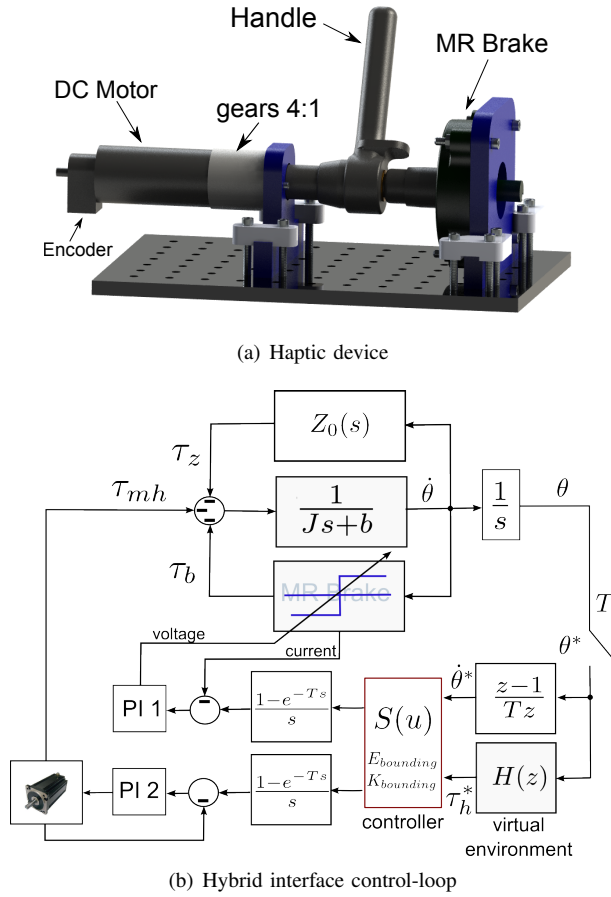


Fig. 7. 1-DOF test bench used to validate the control laws 7(a) comprising a MR brake and a motor and its control scheme 7(b). The current of both actuators are regulated by two analog proportional-integral controllers (PI 1 and PI 2). The brake generates both a controllable torque and a viscous torque, and the braking torque is modelled using Karnopp's stick-slip model.

reference torque until its saturation (from (A) to (B) in the second diagram) and then the brake compensates the torque (B). At  $t=1.41$ s the velocity is inverted and the power becomes negative. The brake is turned off (C) and the motor simulates the decompression phase according to the second stiffness (from (C) to (D) but the motor is saturated). At  $t=2.12$ s, the energy of the motor becomes naturally negative ((D) in the energy's diagram). The motor is then turned off and the torque is transferred to the brake until the total dissipation of the created energy (E). A zoomed view of the torque in this region is shown in the third diagram. Note that if the user tries to compress the spring again, the motor can be activated since it represents a dissipative behaviour (as imposed by (11)). Subsequently, the energy of the motor is maintained positive or zero and the interface is guaranteed passive despite the active virtual environment.

### 5.2 Stiffness-Bounding Algorithm

In the second experiment the virtual environment is defined as a high-stiffness angular spring ( $K=85$  Nm/rad) (Fig. 6(b)). This stiffness overtakes the maximal stiffness displayed by the motor under stability conditions fixed at  $k_{lim}=25$  Nm/rad. Thus, the algorithm limits the motor's torque and the brake

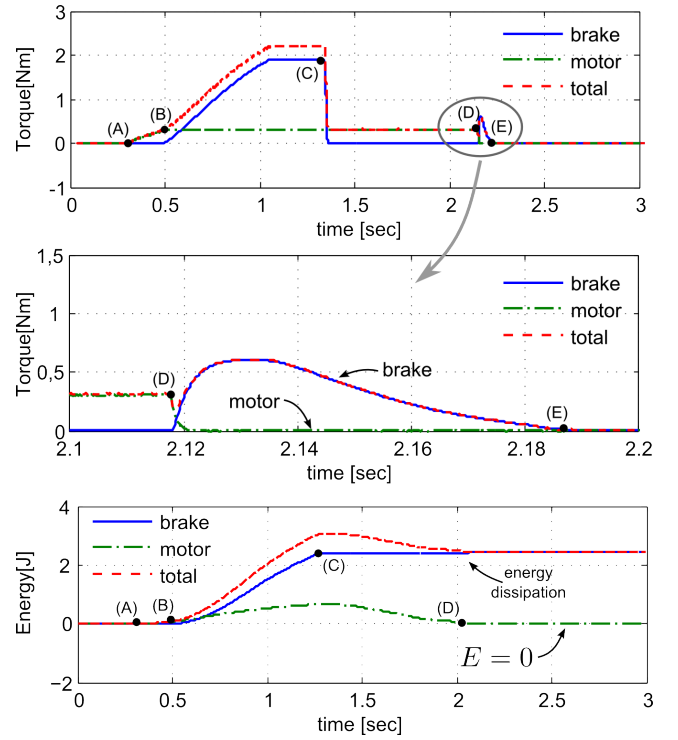


Fig. 8. Experimental results of the simulation of an active virtual environment using the energy-bounding algorithm.

compensates for the difference.

Fig. 9 shows the experimental result. The end effector attains the wall at  $0.26$ rad (A). The algorithm calculates the virtual stiffness and bounds the stiffness sent to the motor to 25 Nm/rad (from (A) to (B)). The difference between the motor's torque and the desired torque is sent to the brake which then displays a stiffness of 60 Nm/rad until the saturation of the motor (B). Beyond this point the total stiffness (85Nm/rad) is transferred to the brake. The reference torque is respected under stability condition using the contribution of the brake and of the motor.

## 6. CONCLUSION

In view of improving both transparency and stability, this paper proposes a control method for an actuator comprising a MR brake and a motor. The sharing of efforts is obtained as a function of the power flow. If the interface dissipates energy, the motor is engaged until its saturation and the brake compensates for the error between the virtual torque and the motor's torque. When the interface restores energy to the operator, the brake is turned off. The coupled system thus behaves equivalently to two independent systems.

A stability analysis has been conducted for this control method. The analysis demonstrated that the system is guaranteed to be passive if the virtual environment is also passive, and assuming greater braking torque capability than the motor's torque. From these results, an energy-bounding based control was implemented to ensure the passivity of the system even for unstable and nonlinear virtual environments. A second stability analysis, via describing function, shows that the stiffness sent to the motor should be limited in order to assure

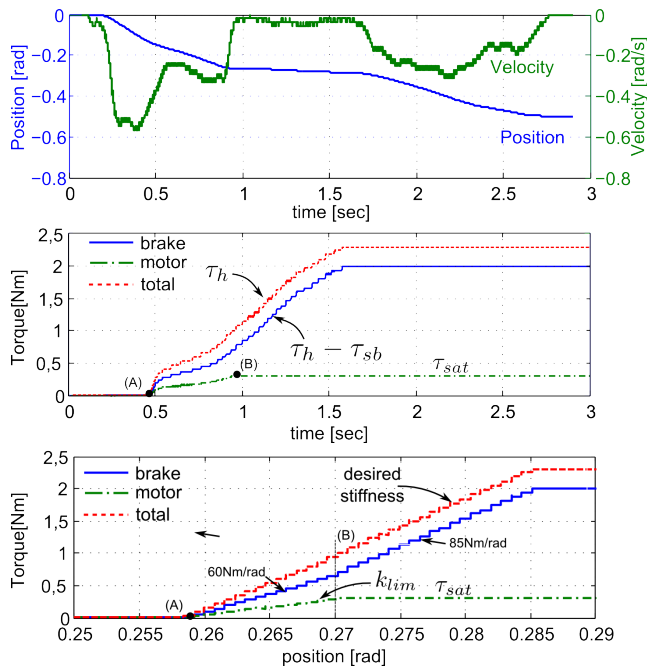


Fig. 9. High-stiffness virtual wall simulation using the stiffness-bounding algorithm. The actuators are engaged with different stiffness values. The segmentation is due to the resolution of the controller to calculate  $\beta(\tau_h)$ .

the passivity of the system. Therefore, a stiffness-bounding algorithm was implemented, which enables the system to simulate an adjustable stiffness between the brake and the motor.

These algorithms work simultaneously. The first one was validated using an active virtual environment. The experimental results demonstrate that the system remains passive. The second one was tested using the simulation of a virtual obstacle. The experimental results demonstrate that the stiffness of the coupled system can be improved under stability constraints. This control method allows the hybrid system to simulate nonlinear and unstable virtual environments and remains independent of the virtual environment model.

## REFERENCES

- [1] J. Colgate and G. Schenkel, "Passivity of a class of sampled-data systems: application to haptic interfaces," in *American Control Conference, 1994*, vol. 3, june-1 july 1994, pp. 3236 – 3240 vol.3.
- [2] J. Colgate and J. Brown, "Factors affecting the z-width of a haptic display," in *1994 IEEE International Conference on Robotics and Automation, 1994. Proceedings*, May 1994, pp. 3205 – 3210 vol.4.
- [3] J. Colgate, M. Stanley, and J. Brown, "Issues in the haptic display of tool use," in *1995 IEEE/RSJ International Conference on Intelligent Robots and Systems 95. 'Human Robot Interaction and Cooperative Robots', Proceedings*, vol. 3, Aug. 1995, pp. 140 – 145 vol.3.
- [4] R. Adams and B. Hannaford, "Stable haptic interaction with virtual environments," *Robotics and Automation, IEEE Transactions on*, vol. 15, no. 3, pp. 465 – 474, jun 1999.
- [5] B. Hannaford and J.-H. Ryu, "Time-domain passivity control of haptic interfaces," *Robotics and Automation, IEEE Transactions on*, vol. 18, no. 1, pp. 1 – 10, feb 2002.
- [6] J.-P. Kim and J. Ryu, "Stable haptic interaction control using energy bounding algorithm," in *Intelligent Robots and Systems, 2004. (IROS 2004). Proceedings. 2004 IEEE/RSJ International Conference on*, vol. 2, sept.-2 oct. 2004, pp. 1210 – 1217 vol.2.

- [7] F. Conti and O. Khatib, "A new actuation approach for haptic interface design," *The International Journal of Robotics Research*, vol. 28, no. 6, pp. 834–848, Jan. 2009.
- [8] C. Rossa, J. Lozada, and A. Micaelli, "A new hybrid actuator approach for force-feedback devices," in *Intelligent Robots and Systems (IROS), 2012 IEEE/RSJ International Conference on*, oct. 2012, pp. 4054 – 4059.
- [9] P. Fauteux, M. Lauria, M.-A. Legault, B. Heintz, and F. Michaud, "Dual differential rheological actuator for robotic interaction tasks," in *Advanced Intelligent Mechatronics, 2009. AIM 2009. IEEE/ASME International Conference on*, july 2009, pp. 47 – 52.
- [10] J. V. Rhijn, "Contribution à l'étude et au développement des systèmes adaptables pour les robots reconfigurables: application à la corobotique," Ph.D. dissertation, INSA Rennes, 2011.
- [11] J. An and D.-S. Kwon, "Stability and performance of haptic interfaces with active/passive actuators: Theory and experiments," *The International Journal of Robotics Research*, vol. 25, no. 11, pp. 1121–1136, Jan. 2006.
- [12] Y.-J. Nam and M.-K. Park, "A hybrid haptic device for wide-ranged force reflection and improved transparency," in *Control, Automation and Systems, 2007. ICCAS '07. International Conference on*, oct. 2007, pp. 1015 – 1020.
- [13] R. B. Gillespie and M. R. Cutkosky, "Stable user-specific haptic rendering of the virtual wall," in *Proceedings of the ASME International Mechanical Engineering Congress and Exhibition*, vol. 58, 1996, p. 397–406.
- [14] J. An and D.-S. Kwon, "In haptics, the influence of the controllable physical damping on stability and performance," in *Intelligent Robots and Systems, 2004. (IROS 2004). Proceedings. 2004 IEEE/RSJ International Conference on*, vol. 2, sept.-2 oct. 2004, pp. 1204 – 1209 vol.2.
- [15] C. Rossa, J. Lozada, and A. Micaelli, "Interaction power flow based control of a 1-dof hybrid haptic interface," in *Haptics: Perception, Devices, Mobility, and Communication*, ser. Lecture Notes in Computer Science, P. Isokoski and J. Springare, Eds. Springer Berlin / Heidelberg, 2012, vol. 7283, pp. 151–156.